Aalborg Universitet

AALBORG UNIVERSITY
DENMARK

Robust Grid-Current-Feedback Resonance Suppression Method for LCL-Type Grid-Connected Inverter Connected to Weak Grid

Zhou, Xiaoping; Zhou, Leming; Chen, Yandong; Shuai, Zhikang; Guerrero, Josep M.; Luo, An; Wu, Wenhua; Yang, Ling

Robust Grid-Current-Feedback Resonance Suppression Method for LCL-Type Grid-Connected Inverter Connected to Weak Grid

Xiaoping Zhou, *Student Member, IEEE*, Leming Zhou, Yandong Chen, *Member, IEEE*, Zhikang Shuai, *Senior Member, IEEE*, Josep M. Guerrero, *Fellow, IEEE*, An Luo, *Senior Member, IEEE*, Wenhua Wu, and Ling Yang

Abstract—In this paper, a robust grid-current-feedback resonance suppression (GCFRS) method for LCL-type grid-connected inverter is proposed to enhance the system damping without introducing the switching noise and eliminate the impact of control delay on system robustness against grid-impedance variation. It is composed of GCFRS method, the full duty-ratio and zero-beat-lag PWM method, and the lead-grid-current-feedback-resonance-suppression (LGCFRS) method. Firstly, the GCFRS is used to suppress the LCL-resonant peak well and avoid introducing the switching noise. Secondly, the proposed full duty-ratio and zero-beat-lag PWM method is used to eliminate the one-beat-lag computation delay without introducing duty cycle limitations. Moreover, it can also realize the smooth switching from positive to negative half-wave of the grid current and improve the waveform quality. Thirdly, the proposed LGCFRS is used to further minimize the control delay and make the positive or negative critical frequency of its virtual equivalent damping resistance increase above 0.5 switching frequency. Then, the system's robustness and dynamic performance can be greatly improved. Finally, the experimental results confirm the theoretical expectations and the effectiveness of the proposed method.

Index Terms—grid-connected inverter; active damping; high-pass filter; control delay; robustness.

I. INTRODUCTION

With the energy crisis and environment problems becoming more and more serious, distributed energy resources (DERs) such as wind and solar power plants are steadily growing [1-2]. As a key device to connect the DERs and utility grid, the grid-connected inverter plays an important role in the distributed power generation systems [3-5]. In the grid-connected inverter, a filter is needed to attenuate the switching harmonics. And the LCL-type output filter is widely adopted due to its better attenuation ability in the high-frequency harmonics than L-type and LC-type filter in the condition of the same amount of total inductance [6-7]. However, LCL-type filter is a low-damping three-order system with resonance problems. Damping solutions must be adopted to stabilize the inverter system [8-9].

Recently, damping solutions for LCL-type filter have been extensively discussed in many literatures, including passive and active damping methods. Compared with passive methods, active ones have drawn considerable attention for its flexible implementation with no extra power losses, including capacitor current feedback [10], capacitor voltage feedback [11], multivariable composite feedback [12], grid current feedback [13-17], and so on. And the grid-current-feedback active damping (GCFAD) method only requires grid-current sensor, which not only reduces the hardware costs, but also improves the system reliability. Especially, the GCFAD method with high-pass-filter (HPF) has drawn much attention for many advantages in engineering applications such as its simple implementation and no noise disturbance [15-17]. However, GCFAD with HPF would introduce the high-order harmonics, especially the switching harmonics and white noise, which will deteriorate the output current waveform. Therefore, an excellent active damping method need be further sought.

Moreover, the impacts of the control delays composed of computation delays and pulse width modulation (PWM) delay should be considering. Reference [18] indicates that the control delay can greatly affects the active damping effect, which could drift the virtual equivalent damping resistance from its designed value. That will drastically deteriorate the stability performance of the control system. For instance, when the LCL-resonance frequency shifts to one-sixth of switching frequency due to the potential influence of the grid impedance, the virtual equivalent damping resistance of capacitor-current-feedback active damping method equals zero at LCL-resonance frequency [19]. Consequently, the digital control system can be hardly stable no matter how much the capacitor-current feedback coefficient is. In addition, this phenomenon similarly exists in other active damping methods (eg. GCFAD) [17]. Therefore, in order to achieve better damping effects and guarantee the stable performance, literature [20]

X. Zhou, L. Zhou, Y. Chen, Z. Shuai, A. Luo, W. Wu, and L. Yang are with the College of Electrical and Information Engineering, Hunan University, Changsha 410082, China (e-mail: zxp2011@hnu.edu.cn; leming_zhou@126.com; yandong_chen@hnu.edu.cn; szk@hnu.edu.cn; an_luo@126.com; wenhua_5@163.com; yangling_1992@163.com).

J. M. Guerrero is with the Department of Energy Technology, Aalborg University, 9220 Aalborg East, Denmark (e-mail: joz@et.aau.dk).

L. Zhou is with the College of Electrical and Information Engineering, Hunan University, Changsha 410082, China (corresponding author, phone: +86-731-88823710; fax: +86-731-88823700; e-mail: leming_zhou@126.com).

indicates that the LCL-filter resonance frequency must keep away from the critical frequency, which causes the virtual equivalent damping resistance to equal zero. However, the LCL-resonance frequency always occurs shifting in practical cases where the impedances variation of long transmission lines and isolation transformers is unavoidable [21-22]. Consequently, the potential instability will be triggered if the grid impedance variation imposes the LCL-resonance frequency migrating to the critical frequency. Therefore, the disturbance-rejection ability (robustness) of the control system against the grid impedance variation cannot be guaranteed [23].

The essential cause of the poor robustness to the grid impedance variation is the inherent control delay, which makes the critical frequency migrate to the design range of LCL-resonance frequency. In order to solve this problem, the following methods can be employed to reduce the control delay, i.e. predictive current control, modifying the sampling instant or PWM method.

The predictive control is usually employed to compensate the control delay, such as neural networks-based estimator [24], fuzzy controller [25], adaptive error correction controller [26], and so on. However, the predictive control is relatively complex, and also introduces additional estimation errors. The control delay can also be reduced by modifying the sampling instant, such as the real-time sampling method [19] and multiple sampling methods [27]. Through shifting the sampling instant toward the PWM reference update instant, the control delay can be reduced. However, restricted by the sampling delay, the duty cycle is unable to vary in full range from 0 to 1. Likewise, modifying sampling way may easily introduce switching ripple and high-frequency switching noise, which could affect normal operation of the control system. Although the proposed two-polarity PWM method in [28] can achieve the full range of duty ratio from 0 to 1, it requires that the total period of A/D sampling and duty-ratio calculation in each switching period is less than a quarter of switching period. Otherwise, the maximum duty ratio will be limited, which make the difficulty of engineering applications increase. What's more, it cannot realize the smooth switching from positive to negative half-wave of the grid current. In order to extend the time duration between the sampling instant and the switching actions, a real-time computation method with dual sampling mode is proposed to remove the computation delay from the inner active damping loop and the outer grid-current control loop simultaneously in [29]. However, because this PWM method is based on the monopole frequency doubling modulation method, which cannot be used in the three-phase inverter system.

For this purpose, a robust grid-current-feedback resonance suppression (GCFRS) method is proposed for the three-phase LCL-type grid-connected inverter connected to weak grid, which can effectively enhance the system damping without introducing the switching noise and eliminate the impact of control delay on system robustness without introducing duty cycle limitations. This paper is organized as follows. Firstly, the model and control method of GCFRS for LCL-type grid-connected inverter is presented in Section II. Then, the robust

GCFRS method for LCL-type grid-connected inverter connected to weak grid is presented in Section III, which is composed of the full duty-ratio and zero-beat-lag PWM method and the lead-grid-current-feedback-resonance-suppression method. To verify the effectiveness of the proposed method, experiments have been carried out in Section IV. Finally, Section V draws the conclusions of this paper.

II. MODEL AND CONTROL METHOD OF GCFRS FOR LCL-TYPE GRID-CONNECTED INVERTER

A. Model and control method of the GCFRS

To suppress the LCL-resonant peak well and avoid introducing the switching noise, the GCFRS method is proposed to control the LCL-type three-phase grid-connected inverter, which is show as Fig. 1. The overall structure of proposed GCFRS method is shown as Fig. 1(a). Wherein, the inductor L_1, L_2 and the capacitor C constitute the LCL filter. R_1 and R_2 are the parasitic resistances of filter inductances L_1 and L_2, respectively. U_{dc} is the input DC voltage; C_{dc} is the DC-link capacitor. Its equivalent single-phase circuit is depicted in Fig. 1(b), wherein u_{inv} and i_L are the inverter output voltage and current, respectively. u_g and i_g are the grid voltage and grid-connected current; L_g is the grid impedance.

Fig.1 (c) shows the control block diagram of the proposed GCFRS method, which is mainly composed of the quasi proportional-resonant (QPR) controller and GCFRS controller. The QPR controller has ability to realize grid current tracking without steady state errors. The GCFRS controller is proposed to damp the LCL-resonance without introducing the switching noise. In addition, the single-current-feedback control method only needs to sample the grid-connected current without extra voltage/current sensors. Then, the hardware cost is reduced, and the system reliability can be also improved. $G(s)$ and $G_v(s)$ represent the transfer functions of QPR controller and GCFRS controller, respectively. Two-polarity PWM modulation is adopted, u_d is the PWM reference signal.

The QPR controller is expressed as [30]:

$$G(s) = K_p + \frac{2K_r\omega_r s}{s^2 + 2\omega_r s + \omega_0^2} \quad (1)$$

where K_p and K_r are the proportional coefficient and resonant gain of QPR controller respectively; ω_r is the cut-off angular frequency of QPR, and ω_0 is the fundamental angular frequency.

The transfer function of GCFRS controller is expressed as

$$G_V(s) = -\frac{R_V}{U_{dc}} \frac{s\omega_V / Q_V}{s^2 + s\omega_V / Q_V + \omega_V^2} \quad (2)$$

where

$$\begin{cases} \omega_V = \sqrt{\omega_L\omega_H} \\ Q_V = \sqrt{\omega_L\omega_H} / (\omega_L + \omega_H) \end{cases} \quad (3)$$

In (2) and (3), the cutoff angular frequency ω_L is used to obtain the main component of i_L around the resonance angular frequency ω_{res}; ω_H is used to avoid introducing the switching noise; the virtual resistance R_V is desired to add the damper for LCL filter.
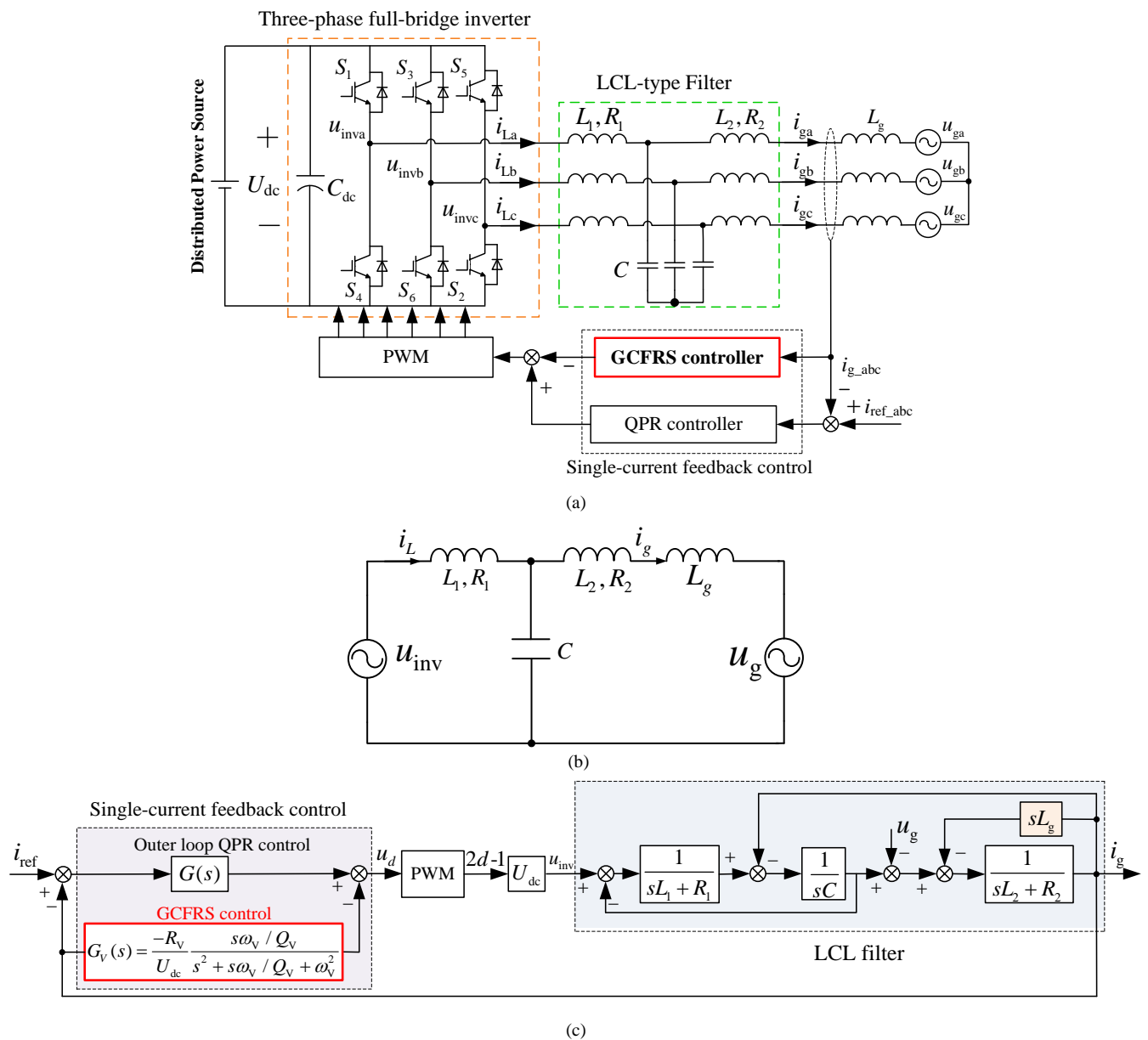
Fig.1. Configuration of the proposed GCFRS for LCL-type grid-connected inverter. (a) The overall structure of proposed GCFRS method. (b) Equivalent single-phase circuit. (c) Control block diagram of the proposed GCFRS method.

From Fig.1 (c), the transfer function between $i_g(s)$ and $u_{inv}(s)$ can be expressed as:

$$Y_g(s) = \frac{i_g}{u_{inv}} = \frac{1}{L_1(L_2 + L_g)Cs[s^2 + \omega_{res}^2]} \tag{4}$$

where ω_{res} is the resonance angular frequency of the LCL filter, given by:

$$\omega_{res} = \sqrt{\frac{L_1 + L_2 + L_g}{L_1(L_2 + L_g)C}} \tag{5}$$

B. Equivalent impedance property analysis of the proposed GCFRS method in the digital control

With the traditional PWM method in the digital control, the grid current is sampled at the initial of each switching period. If the duty-ratio d is loaded in the present switching period, d cannot achieve a full range (0~1) due to the computation time

T_d (eg. A/D sampling and duty-ratio calculating time). As a result, it will affect the output quality of grid-current waveform. Therefore, d is usually loaded in the next switching period in the digital control, where the computation delay is expressed as:

$$G_{delay}(s) = e^{-sT_s} \tag{6}$$

where T_s is the sampling period. In addition, the control delay caused by zero-order hold in the digital control is modeled as [22]:

$$G_h(s) = \frac{1 - e^{-sT_s}}{s} \tag{7}$$

From (6) and (7), the control delay of inverter in the digital control can be derived as:

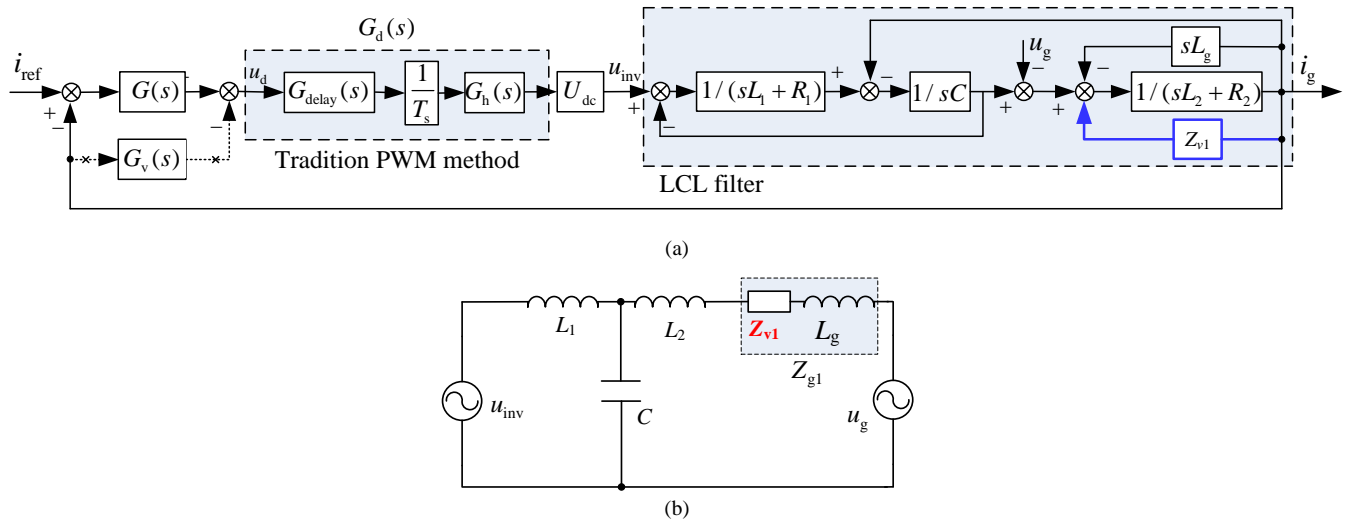$$G_d(s) = G_{delay}(s)G_h(s) / T_s \tag{8}$$

Fig.2. (a) The equivalent control diagram in the digital control with traditional PWM control method. (b) Equivalent impedance of GCFRS.

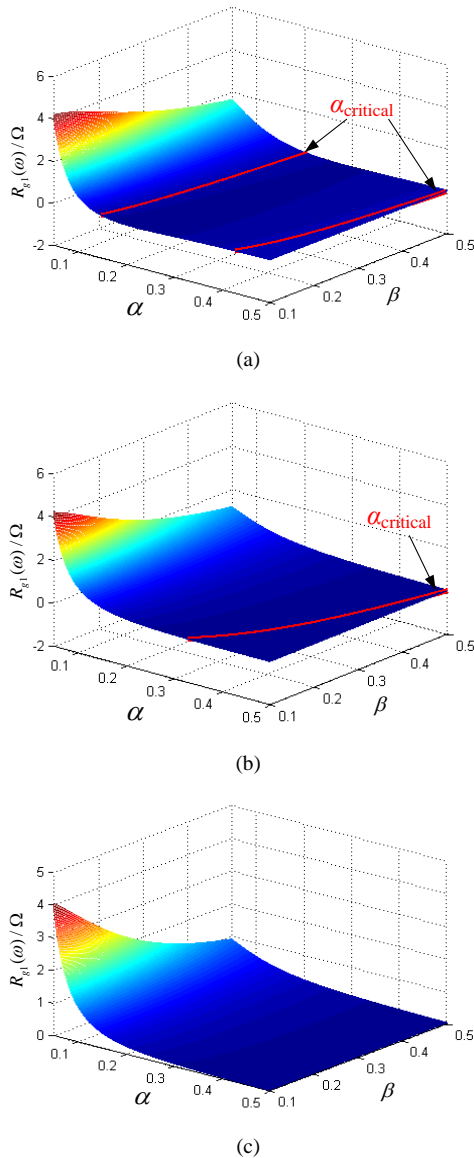Fig.3 Frequency-domain characteristics of $R_{g1}(\omega)$ vary with β under different control-delay conditions. (a) λ=1.5. (b) λ=0.5. (b) λ=0.

By substituting s=$j\omega$ into (8), the expression can be obtained as:

$$G_d(j\omega) = \frac{2\sin(0.5\omega T_s)}{\omega T_s}e^{-1.5j\omega T_s} \quad (9)$$

From (9), it is noted that the control delay with the traditional PWM method in the digital control is 1.5 times sampling period.

To analyze the equivalent impedance property of the proposed GCFRS method in the digital control, an equivalent control diagram is derived in Fig. 2 (a). While shifting the feedback path of $G_v(s)$ to the input of the transfer function $1/(sL_2+R_2)$, it is equivalent to a virtual impedance Z_{v1} connected in series between inductance L_2 and grid inductance L_g, as shown in Fig.2 (b), where the dotted line is replaced by the blue solid line. Ignoring the parasitic resistances R_1 and R_2, the expression of Z_{v1} can be derived in (10).

$$Z_{v1} = \frac{G_v(s)G_d(s)U_{dc}}{s^2 L_1 C} \quad (10)$$

In order to facilitate the analysis of the effect of control delay on the impedance property of the proposed GCFRS method. the control delay is defined as λT_s. Thus, the expression of control delay can be rewritten as:

$$G_d(j\omega) = \frac{2\sin(0.5\omega T_s)}{\omega T_s}e^{-\lambda j\omega T_s} \quad (11)$$

Taking Z_{v1} and sL_g together, the equivalent connection impedance Z_{g1} can be expressed as:

$$Z_{g1} = Z_{v1} + sL_g \quad (12)$$

Substituting s=$j\omega$ into (12), the expression of $Z_{g1}(j\omega)$ can be derived as:

$$Z_{g1}(\omega) = j\omega L_g + \frac{2R_V\omega_V\sin(0.5\omega T_s)[\cos(\lambda\omega T_s) - j\sin(\lambda\omega T_s)]}{\omega_V T_s L_1 C\omega^3 - j(T_s L_1 C Q_V \omega_V^2\omega^2 - T_s L_1 C Q_V \omega^4)} \quad (13)$$

where, $Z_{g1}(\omega)$ can be considered as the equivalent damping resistance $R_{g1}(\omega)$ connected in series with the equivalent reactance $X_{g1}(\omega)$:

$$Z_v(\omega) = R_{g1}(\omega) + jX_{g1}(\omega) \quad (14)$$

where $R_{g1}(\omega)$ and $X_{g1}(\omega)$ are expressed as:

$$\begin{cases} R_{g1}(\omega) = \dfrac{AD}{B^2+D^2}\sin(\lambda\omega T_s) - \dfrac{AB}{B^2+D^2}\cos(\lambda\omega T_s) \\ X_{g1}(\omega) = \dfrac{AD}{B^2+D^2}\cos(\lambda\omega T_s) + \dfrac{AB}{B^2+D^2}\sin(\lambda\omega T_s) + \omega L_g \end{cases} \quad (15)$$

where,

$$\begin{cases} A = 2R_V\omega_V\sin(0.5\omega T_s) \\ B = \omega_V T_s L_1 C\omega^3 \\ D = T_s L_1 C Q_V \omega_V^2 \omega^2 - T_s L_1 C Q_V \omega^4 \end{cases} \quad (16)$$

From (15), the frequency characteristics of $R_{g1}(\omega)$ varying with β under different control delay conditions are drawn in Fig.3, where f_s is the switching frequency; α is defined as $\omega/(2\pi f_s)$; $\alpha_{critical}$ is the positive or negative critical frequency of $R_{g1}(\omega)$; β is defined as $\omega_V/(2\pi f_s)$. As shown in Fig.3 (a) and (b), when $\lambda=1.5$ or 0.5, $\alpha_{critical}$ is located in the LCL-resonant frequency design range of $\alpha<0.5$. Then, the grid-inductance variation could impose the LCL-resonant frequency ω_{res} migrating to the critical point $\alpha_{critical}$, and $R_{g1}(\omega)$ can't maintain positive damping characteristic at ω_{res}, especially while $R_{g1}(\omega)$ is equal to 0 at ω_{res}, the system can hardly maintain stable[18-20]. Hence, the stability problem can be aroused by grid inductance under the weak grid condition. While $\lambda=0$, $R_{g1}(\omega)$ maintains positive damping characteristic all along during the LCL-resonance frequency range, as shown in Fig.3(c). Thus, a good resonant suppression effect and stability can be guaranteed regardless of the grid-inductance variation. However, for the traditional PWM algorithm, its computation delay is T_s and the control delay is $1.5T_s$ ($\lambda=1.5$). In this case, the robustness of inverter against grid impedance is poor.

III. ROBUST GCFRS METHOD FOR LCL-TYPE GRID-CONNECTED INVERTER CONNECTED TO WEAK GRID

According to the section II, the essential cause of the poor robustness against grid impedance variation is the inherent control delay, which makes the critical frequency of the virtual equivalent damping resistance be located in the design range of LCL-resonance frequency. To improve the system robustness against wide variation of L_g, the robust GCFRS method is proposed for active damping loop to reduce the control delay and design $\alpha_{critical}>0.5$, which is shown in Fig. 4. It is composed of the full duty-ratio and zero-beat-lag PWM method and lead-grid-current- feedback-resonance-suppression (LGCFRS).

A. Full duty-ratio and zero-beat-lag PWM method

The full duty-ratio and zero-beat-lag PWM method is proposed to eliminate the one-beat-lag computation delay without introducing duty cycle limitations, which is shown as Fig. 5. The proposed PWM method can be implemented in two stages as shown in Fig. 5 (a). The initial stage: Considering program initialization, the current duty-ratio cannot be calculated firstly, and it is loaded on the valley of next carrier. The second stage: The duty-ratio will be loaded twice in each switching period, which is instantaneously updated at the peak and valley of the carrier, respectively. At the beginning of each

switching period, the duty-ratio is updated firstly. Then, during the first half of the switching period, the A/D sampling and duty-ratio calculation are executed preferentially to calculate the pulse width in current switching period ($T_d\leq0.5T_s$). After a lapse of $0.5T_s$ duration, the duty-ratio is updated once again to make the pulse width equal the calculated value, as shown in Fig. 5 (a). T_b is the time of the liquid-crystal display and RMS calculation. Actually, since the liquid-crystal display and RMS calculation have occupied much time in each switching period, the computation time T_d of A/D sampling and duty-ratio with a large duration of $0.5T_s$ is enough for most applications, even for a high switching frequency.

This paragraph depicts the concrete implementation process of the second stage. Taking the $(k+1)^{th}$ switching period as an example, as shown in Fig. 5(a). 1) At the instant t_1, the value of pulse width is updated first to be $T_s d(k)$, where $d(k)$ is the duty-ratio in the previous k^{th} switching period. Therefore, the pulse width during the half of $(k+1)^{th}$ switching period will be $0.5T_s d(k)$. 2) At the instant t_2, the PWM reference signal u_d equals the value of current carrier u_{tri}, and the switching action is triggered. 3) At the instant t_3, the duty-ratio of the current $(k+1)^{th}$ switching period is calculated as $d(k+1)$. 4) At the instant t_4, the pulse width is updated once again to make the pulse width of the $(k+1)^{th}$ switching period equal the calculated value $T_s d(k+1)$, where the second instantaneous updated duty-ratio is defined as $D(k+1)$. Therefore, the pulse width of the second half switching period should be adjusted to $T_s d(k+1)-0.5T_s d(k)$. Meanwhile, considering the triangular carrier is symmetrical, the duty-ratio $D(k+1)$ will be set as $2[d(k+1)-0.5d(k)]$. 5) At the instant t_5, the switching action is triggered once again.

Similarly, for any $(k+i)$ $(i=2,3,4,\ldots)$ switching period, the duty-ratio expression of $D_a(k+i)$ and $D(k+i)$ is expressed as Eq.(17) and Eq.(18), where $D_a(k+i)$ is the first updated duty-ratio in the $(k+i)^{th}$ switching period, and $D(k+i)$ is the second updated duty-ratio in the $(k+i)^{th}$ switching period.

$$\begin{cases} D_a(k+1) = d(k) \\ D_a(k+i) = D(k+i-1) \quad i=2,3,4\cdots \end{cases} \quad (17)$$

$$\begin{cases} D(k+1) = 2[d(k+1)-0.5d(k)] \\ D(k+i) = 2[d(k+i)-0.5D_a(k+i)] \quad i=2,3,4\cdots \end{cases} \quad (18)$$

However, due to $0\leq D(k+i)\leq1$, the duty-ratio $d(k+i)$ in the $(k+i)^{th}$ switching period should meet the following conditions.

$$0.5D(k+i-1) \leq d(k+i) \leq 0.5+0.5D(k+i-1) \quad (19)$$

From (19), it is noted that $d(k+i)$ is limited by the previous updated duty-ratio $D(k+i-1)$. For example, if the grid-current wave is located in the negative half period, d cannot achieve the range between 0~0.5, as shown in Fig. 6 (a). In contrast, if the grid-current wave is located in the positive half period, d cannot achieve the full range between 0.5~1, as shown in Fig. 6 (b). Therefore, d cannot achieve the full range (0 to 1) due to (19). And that may make the condition of (17) difficult to meet (19) in the transient operation, such as system mutation from half load to full load, or vice versa. Under such circumstance, system might take more switching period to convert
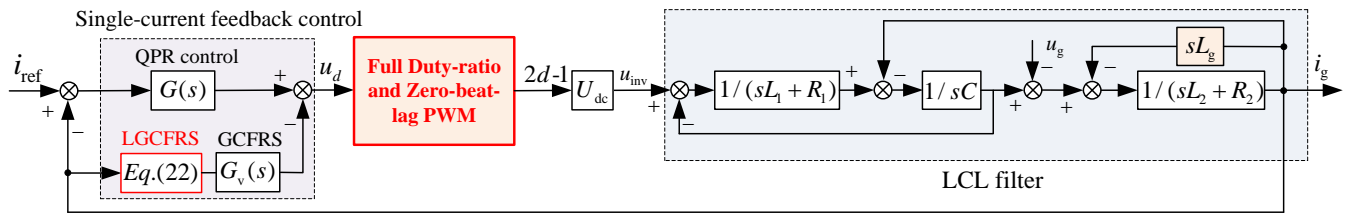
Fig.4. Control block diagram of the robust GCFRS for LCL-type grid-connected inverter in the equivalent continuous-time domain.
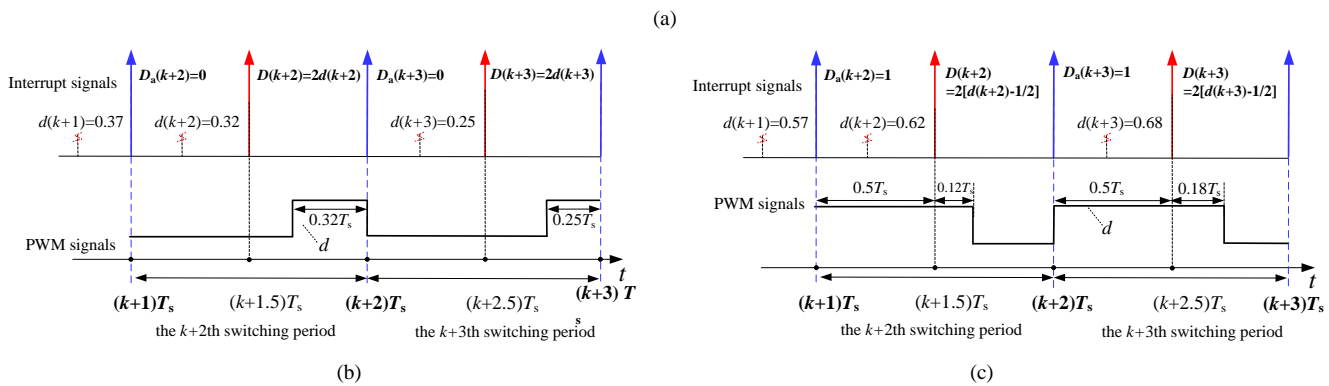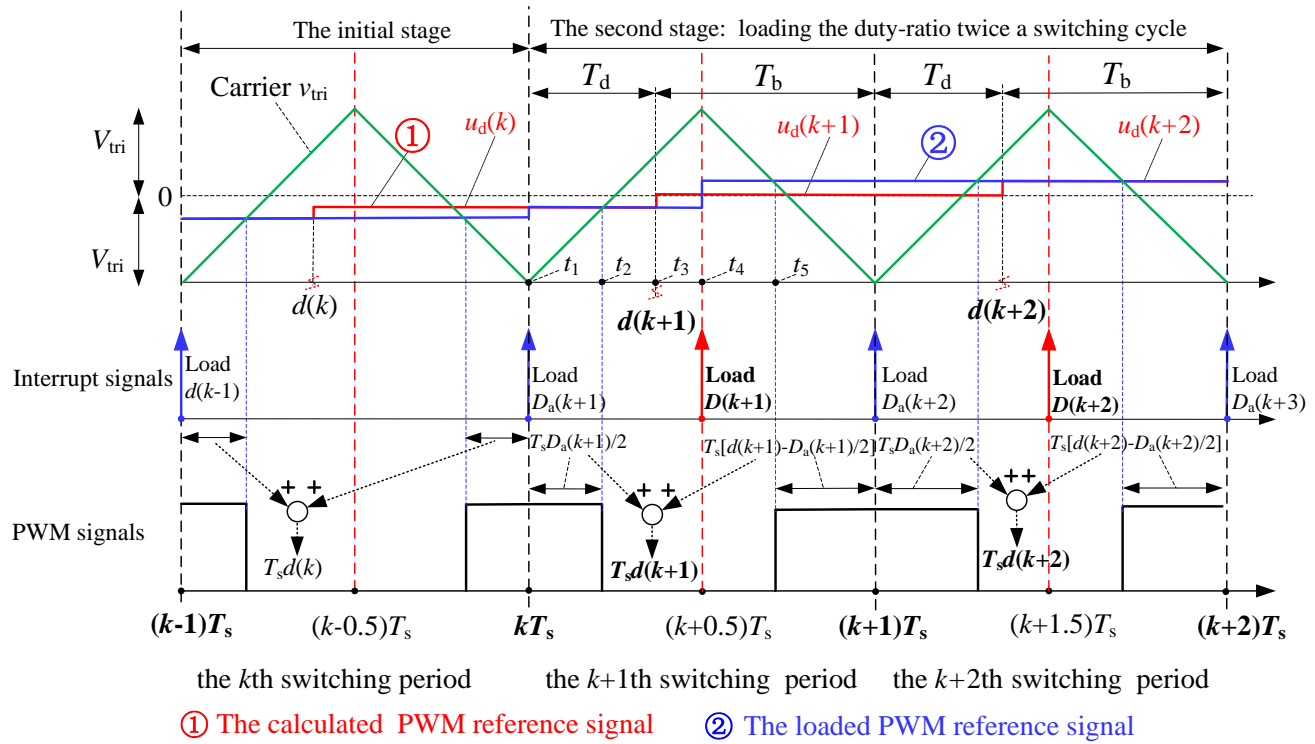

① The calculated PWM reference signal   ② The loaded PWM reference signal

(a)

(b)

(c)

Fig. 5. The design scheme of full duty-ratio and zero-beat-lag PWM method. (a)Without considering of full duty ratio or case B. (b) Case A. (c) Case C.

Table.1 The design value of $D_a(k+i)$

	Conditions	$D_a(k+i)$
Case A	$d(k+i-1)<0.5-\Delta d_{opt}$	0
Case B	$0.5-\Delta d_{opt} \leq d(k+i-1)\leq 0.5+\Delta d_{opt}$	Eq.(17)
Case C	$d(k+i-1)> 0.5+\Delta d_{opt}$	1

from transient-state to steady state, which results in a poor system dynamics. Therefore, in order to eliminate the restrictions of $D(k+i-1)$ on $d(k+i)$, the updated value of $D_a(k+i)$

is reset to eliminate the coupling between $D(k+i-1)$ and $d(k+i)$, which is shown in Table.1

From Table.1, setting $D_a(k+i)=0$ when the grid-current is in the negative half period, then the range of duty-ratio $d(k+i)$ will be within the interval (0~0.5), as shown in Fig. 5 (b). Moreover, setting $D_a(k+i)=1$ when the grid-current is in the positive half period, then the range of duty-ratio $d(k+i)$ will be within the interval (0.5~1), as shown in Fig. 5 (c). With these extensions, the limitation of (19) is eliminated, and the full range of duty-ratio (0~1) is achieved, as shown in Fig. 6 (c).
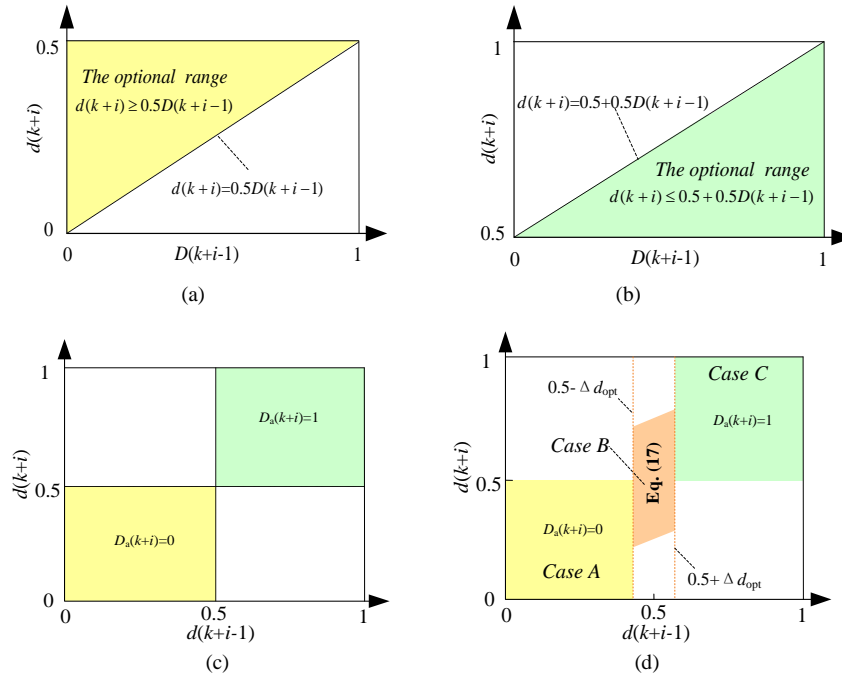
Fig. 6. The range of duty-ratio with different design value of $D_a(k+i)$. (a) $Eq.(17)$ in the negative half period. (b) $Eq.(17)$ in the positive half period. (c)The design value for full duty-ratio.(d) The finally proposed design method for $D_a(k+i)$.

However, the abovementioned method in Fig. 6 (c) may not be satisfied when duty-ratio is closed to 0.5. For example, with $d(k+i-1)=0.502$ and $d(k+i)=0.498$, it is difficult to realize the smooth switching from positive to negative half-wave due to $D_a(k+i)=1$ at this time. Therefore, when the $d(k+i-1)$ is in the range between $0.5-\Delta d_{opt}$ and $0.5+\Delta d_{opt}$ (closes to 0.5), $D_a(k+i)$ is further designed to be updated with the (17) to facility the smooth switching of positive and negative output grid-current wave, as shown in Fig. 6 (d), where Δd_{opt} is a small offset value. Though it cannot achieve the full duty-ratio in the range between $0.5-\Delta d_{opt}$ and $0.5+\Delta d_{opt}$, the proposed PWM method can still provide a range of allowable duty-ratio for both steady and transient state because this region does not need too high or too low duty-ratio.

B.   LGCFRS Method

From section III.A, it is noted that the control delay of the proposed full duty-ratio and zero-beat-lag PWM method is only $0.5T_s$ due to the computation delay is eliminated. However, $\alpha_{critical}$ is still located in the resonant frequency design range. For this purpose, the LGCFRS method with adding a lead-control part is further proposed to minimize the control delay and make $\alpha_{critical}$ increase above 0.5, where the lead-control part is preliminary designed as $e^{\zeta sTs/2}$, and ζ is the lead-control coefficient.

Make $e^{\zeta sTs/2}$ be expanded with Taylor series.

$$e^{\zeta sT_s/2} = 1 + s \cdot (\zeta T_s / 2) + \left[s \cdot (\zeta T_s / 2) \right]^2 / 2! + \cdots \quad (20)$$

In the digital control, the Taylor series can be approximated by using the difference equation. Then, while considering the first three series of Taylor series in (20), the transfer function $G_L(z)$ of LGCFRS in the z-domain can be derived to (21).

$$G_L(z) = 0.5\zeta^2 + \zeta + 1 - \zeta(\zeta+1)z^{-0.5} + 0.5\zeta^2 z^{-1} \quad (21)$$

Taking $z^{-0.5} = e^{-sTs/2}$ and $z^{-1} = e^{-sTs}$, the transfer function $G_L(s)$ of LGCFRS in s-domain is expressed as follows.

$$G_L(s) = 0.5\zeta^2 + \zeta + 1 - \underbrace{\zeta(\zeta+1)e^{-sT_s/2} + 0.5\zeta^2 e^{-sT_s}}_{\text{the lead-control part}} \quad (22)$$

Combining the full duty-ratio and zero-beat-lag PWM method and LGCFRS, the frequency-domain characteristic of virtual resistance $R_{g1}(\omega)$ has largely changed. Fig.7 depicts the values of $\alpha_{critical}$ with different ζ under robust GCFRS control. Obviously, while $\zeta \geq 1$, $\alpha_{critical}$ could increase above 0.5 regardless of ω_V variation, and then $R_{g1}(\omega)$ presents positive in the interval of $(0, 0.5)$ all along. Therefore, the LCL-type grid-connected inverter could have a good robustness against grid impedance variation at this time. For the convenience of calculation, the value of ζ is 1 in this paper.
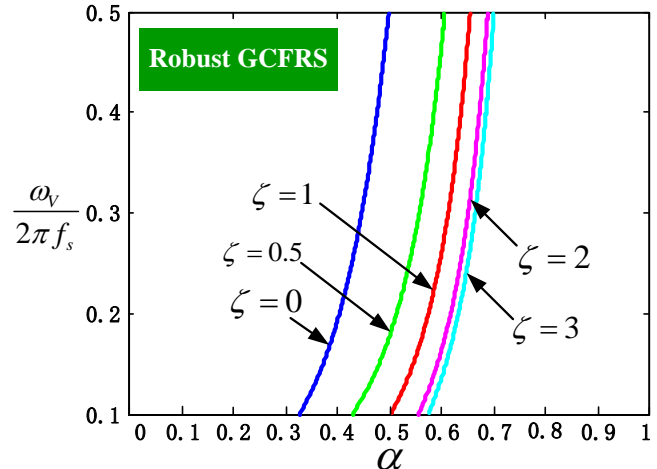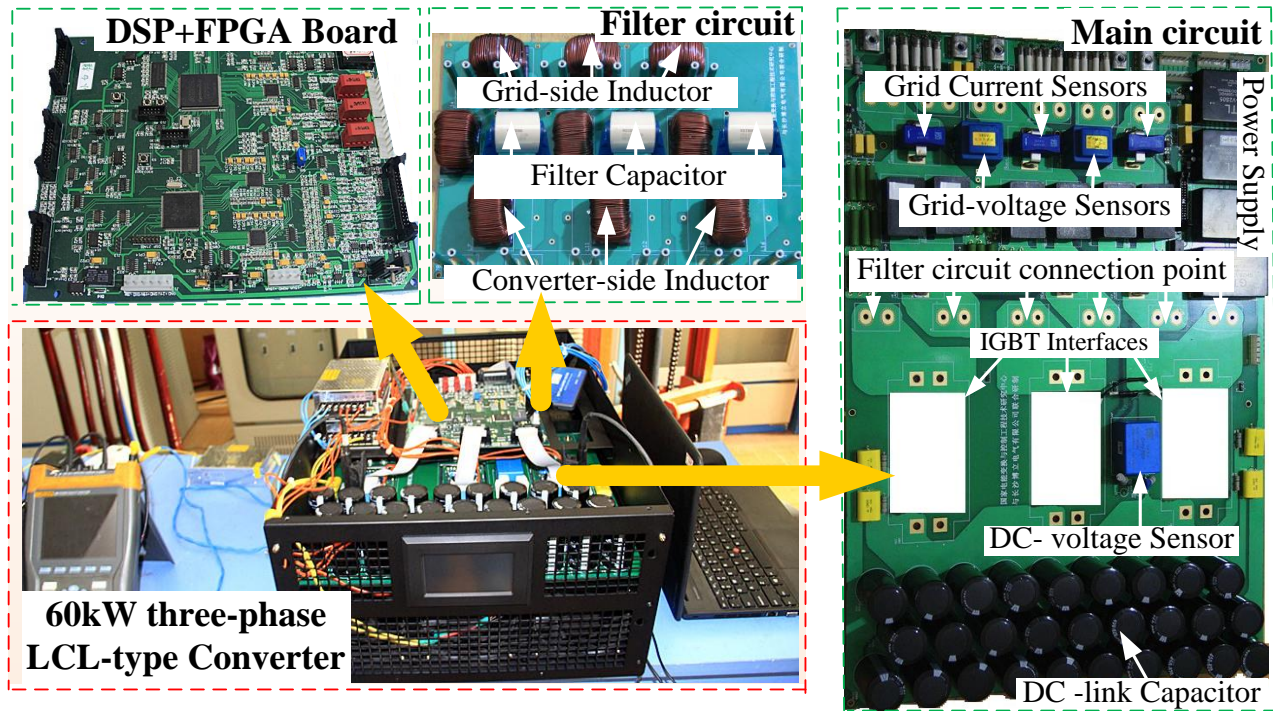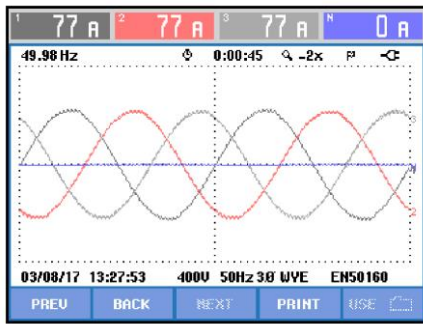

Fig.7. the values of $\alpha_{critical}$ with different ζ under robust GCFRS control.
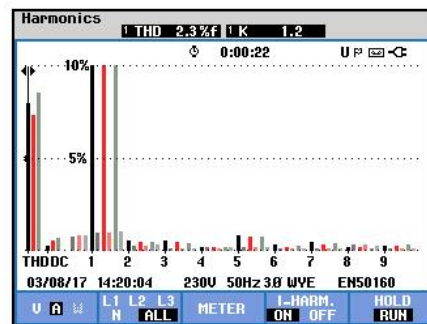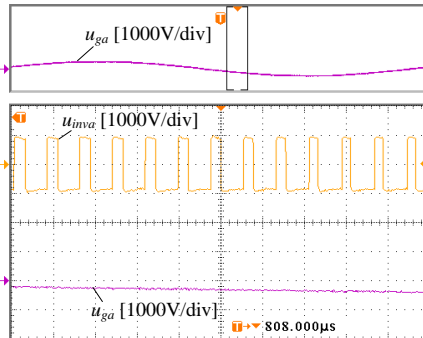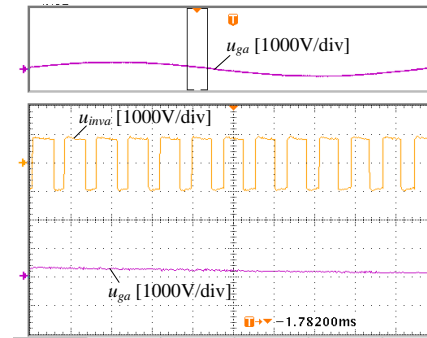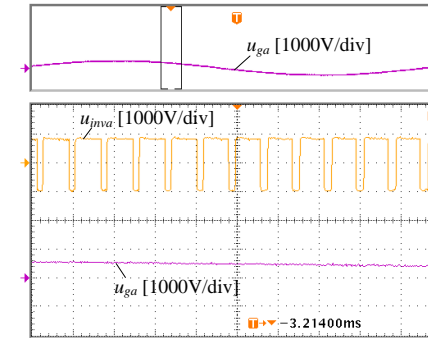
Fig.8. (a) Prototype of 60kW three-phase LCL-type grid-connected inverter. (b) The grid current waveform under full load condition. (c)The THD of grid current under full load condition. (d)The power factor of grid current under full load condition. (e)The experimental inverter output-voltage waveform in case A. (f) The experimental inverter output-voltage waveform in case B.(g) The experimental inverter output-voltage waveform in case C.

IV. EXPERIMENTAL VERIFICATION

To verify the validity of the proposed control method, a 60kW three-phase LCL-type inverter prototype has been built in the laboratory, as shown in Fig.8 (a). IPM module FF300R17ME4 is selected as the power device. AD7656 is used as the sampling chip. Prototype parameters are shown in Table.2. The experiment shows that the total time for A/D sampling and calculation is 7.3us; the time for the grid current outer loop QPR control is 6.3us, the time for the LGCFRS control is 6.1us, and the time for the inner loop GCFRS control is 4.6us. When the sampling frequency is 12.8 kHz, the time requirement for A/D sampling and duty-ratio calculating only accounts for 31% of switching period, which is less than half of switching period.

Fig.9. (a) the dynamic experimental waveform of grid-current from half-load to full-load when inverter adopts the GCFRS method with the symmetrical PWM method. (b) The dynamic experimental waveform of grid-current from half-load to full-load when inverter adopts the GCFRS with the proposed full duty-ratio and zero-beat-lag PWM method. (c) The dynamic experimental waveform of grid-current from half-load to full-load when inverter adopts the proposed robust GCFRS method. (d) Steady state experimental results in weak grid wh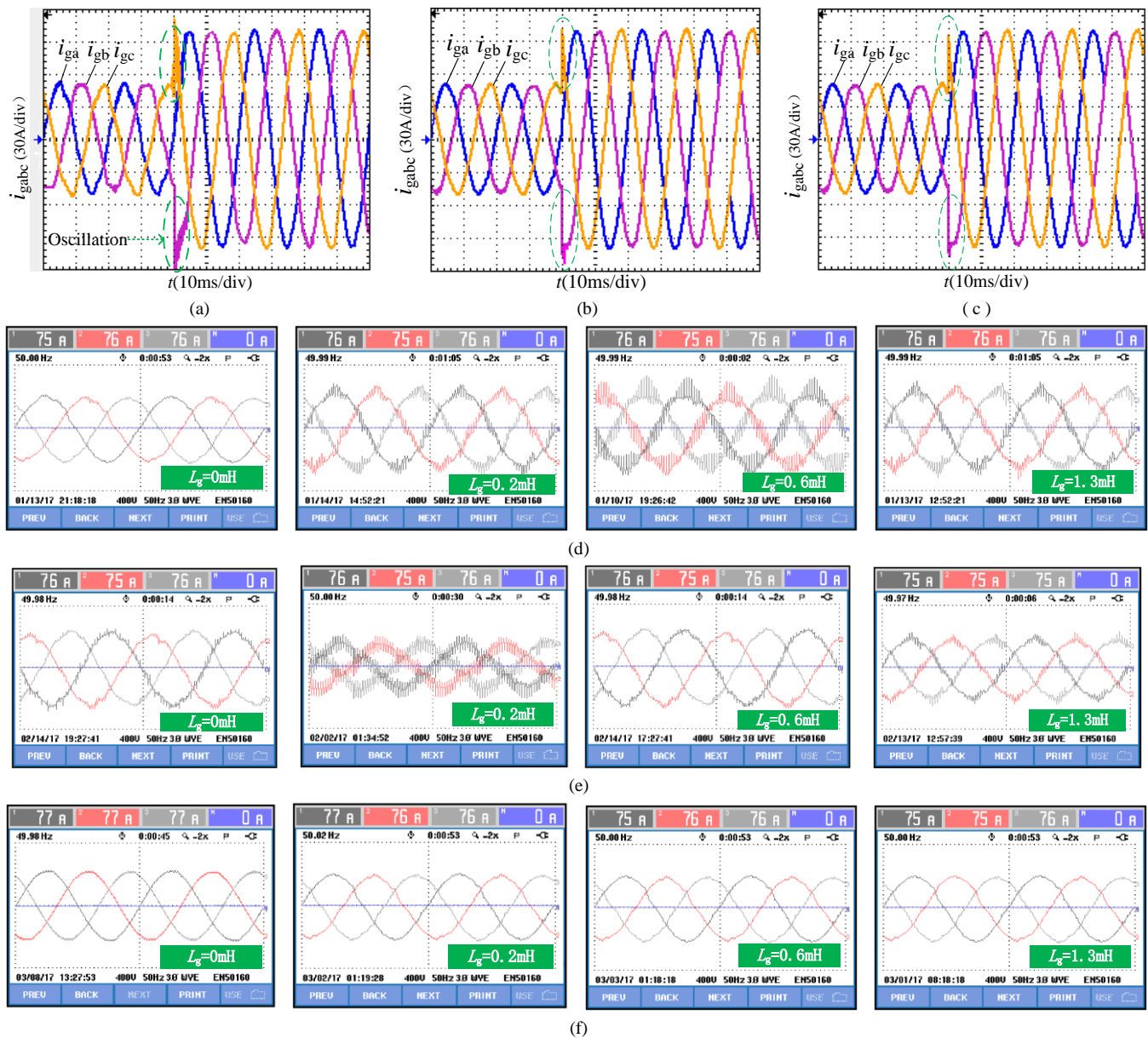en inverter adopts the GCFRS method with the symmetrical PWM method. (e) Steady state experimental results in weak grid when inverter adopts the GCFRS with the proposed full duty-ratio and zero-beat-lag PWM method. (f) Steady state experimental results in weak grid when inverter adopts the proposed robust GCFRS method.

Fig.8 (b), (c) and (d) show the experimental results of grid current waveform, total harmonic distortion (THD), and power factor (PF) under full load condition by using the proposed robust GCFRS method. We can see that the PF reaches 1, and the THD is only 2.3%. It is less than the national standard of 5%, which verifies the proposed robust GCFRS method can inject higher quality active power into the grid.

Fig.8 (e)-(g) display the experimental waveforms of inverter output-voltage in case A, case B, and case C, respectively. Due to the synchronization between the grid-current and grid-voltage, the zero crossing point from negative half of grid-current wave to positive one can be obtained by zero-crossing capture of grid-voltage. Moreover, the negative and positive half-wave of grid current occupy 0.5N (N=f_s/f_0) times switch-

ing period respectively, where f_0 is the fundamental frequency of grid voltage. Therefore, $D_a(k+i)$ equals 0 when the grid-current wave is within the interval of (0.55N~0.95N) times switching period, as seen in Fig.8 (e). $D_a(k+i)$ equals 1 when the grid- current wave is within the interval of (0.05N~0.45N) times switching period, as seen in Fig.8 (g). $D_a(k+i)$ equals (17) for smooth handoff when the grid- current wave is within the interval of [0~0.05N], [0.45N~0.55N], [0.95N~N] times switching period, as seen in Fig.8 (f).

Fig.9 (a)-(c) display the contrastive dynamic experimental waveforms of grid-current from half-load to full-load among the GCFRS method, the GCFRS with the proposed full duty-ratio and zero-beat-lag PWM method, and the proposed robust GCFRS method. As we can see from the Fig.9 (a)-(c), by

using the proposed robust GCFRS method, the waveform of grid current keeps a stable operation and responds quickly when the grid-current is from half-load to full-load, as shown in Fig.9 (c). In addition, the proposed robust GCFRS method has faster response speed, smaller overshoot and better dynamic performance compared with other two methods.

Table.2 System parameters

Parameter	Value	Parameter	Value
K_p	0.03	U_{dc}/V	700
K_r	2	L_1/mH	0.7
ω_r	π	L_2/mH	0.2
T_s/s	1/12800	R_1/Ω	0.16
ω_0	314.159	R_2/Ω	0.09
u_g/V	220	C/μF	10
ω_v/(10^4rad/s)	2.1	C_{dc}/μF	5740
Q_v	0.24	ζ	1
R_v	1	P/kW	60

In order to simulate the effect of grid impedance in weak grid on LCL-type inverter, the contrastive experiments have been conducted in which inductances are connected in series to the right of the line-side resistance L_2. Fig.9 (d)-(f) display the contrastive experimental results among the GCFRS method, the GCFRS with the proposed full duty-ratio and zero-beat-lag PWM method, and the proposed robust GCFRS method when grid impedance takes different values. As can be seen from Fig.9 (d)-(e), when inverter adopts the GCFRS method or the GCFRS with the proposed full duty-ratio and zero-beat-lag PWM method, the grid current has gradual oscillations with the changes of L_g, especially when actual resonance frequency is closed to the critical frequency of equivalent impedance (L_g=0.6mH at Fig.9(d), L_g=0.2mH at Fig.9(e)). However, when inverter adopts the proposed robust GCFRS method, the equivalent damping resistance shows its positive resistance feature at the actual resonance frequency. The grid current waveform is smooth, as shown in Fig.9(f). The contrastive experimental results verify that the proposed robust GCFRS method can effectively suppress the influence of grid impedance on the inverter control, and improve the robustness of LCL-type inverter against the L_g variation in the weak grid.

V. CONCLUSION

In this paper, a robust grid-current-feedback resonance suppression (GCFRS) method is proposed for the three-phase LCL-type grid-connected inverter connected to weak grid, which can effectively enhance the system damping without introducing the switching noise and eliminate the impact of control delay on system robustness against grid-impedance variation. Based on the theoretical analysis, and experimental evaluation, we can conclude that:

1) The proposed GCFRS can effectively suppress the LCL-resonant peak well and avoid introducing the switching noise

2) Due to the inherent control delay in the digital control, the critical frequency of the virtual equivalent damping resistance is located in the LCL-resonant frequency design range of α<0.5. Therefore, the wide-range variation of grid impedance is most likely to affect the stable performance of inverter.

3) The proposed full duty-ratio and zero-beat-lag PWM method can effectively eliminate the one-beat-lag computation delay without introducing duty cycle limitations, which improves the stable and dynamic performance of inverter system. Moreover, it can also realize the smooth switching from positive to negative half-wave of the grid current and improve the waveform quality.

4) Half of switching period for A/D sampling and duty cycle calculation is allowed in the proposed full duty-ratio and zero-beat-lag PWM method, which reduces the difficulty of engineering implementations.

5) The proposed LGCFRS can further minimize the control delay and make the critical frequency of the virtual equivalent damping resistance increase above 0.5 switching frequency. Then, the system's robustness and dynamic performance can be greatly improved.

REFERENCE

[1] Z. K. Shuai, W. Huang, C. Shen, J. Ge, and Z. J. Shen, "Characteristics and restraining method of fast transient inrush fault currents in synchronverters," *IEEE Trans. Ind. Electron.*, vol. 64, no. 9, pp.7487-7497, Sep. 2017.

[2] Z. K. Shuai, C. Shen, X. Yin, X. Liu, and Z. J. Shen, "Fault analysis of inverter-interfaced distributed generators with different control schemes," *IEEE Transactions on Power Delivery,* DOI: 10.1109/ TPWRD.2017.2717388.

[3] F. Blaabjerg, R. Teodorescu, M. Liserre, and A. V. Timbus, "Overview of control and grid synchronization for distributed power generation systems," *IEEE Trans. Ind. Electron.*, vol. 53, no. 5, pp. 1398-1409, Oct. 2006.

[4] S. E. C. Dos, C. B. Jacobina, N. Rocha, J. A. A. Dias, and M. B. R. Correa, "Single-phase to three-phase four-leg converter applied to distributed generation system," *IET Power Electron.*, vol. 3, no. 6, pp. 892-903, Nov. 2010.

[5] Z. K. Shuai, Y. Hu, Y. L. Peng, C. M. Tu, and Z. J. Shen, "Dynamic stability analysis of synchronverter-dominated microgrid based on bifurcation theory," *IEEE Trans. Ind. Electron.*, vol. 64, no. 9, pp.7467-7477, Sep. 2017.

[6] Y. R. Mohamed, M. Rahman, and R. Seethapathy, "Robust line-voltage sensorless control and synchronization of LCL-filtered distributed generation inverters for high power quality grid connection," *IEEE Trans. Power Electron.*, vol. 27, no. 1, pp. 87-98, Jan. 2012.

[7] A. Ghoshal, and V. John, "Active daming of LCL filter at low switching to resonance frequency ratio," *IET Power Electron.*, vol. 8, no.4, pp. 574-582, Apr. 2015.

[8] S. Zhang, S. Jiang, X. Lu, B. Ge, and F. Z. Peng, "Resonance issues and damping techniques for grid-connected inverters with long transmission cable," *IEEE Trans. Power Electron.*, vol. 29, no.1, pp. 110–120, Jan. 2014.

[9] M. Hanif, V. Khadkikar, W. Xiao, and J. L. Kirtley, "Two degrees of freedom active damping technique for LCL filter-based grid connected PV systems," *IEEE Trans. Ind. Electron.*, vol.61, no. 6, pp. 2795–2803, Jun. 2014.

[10] M. Wagner, T. Barth, R. Alvarez, C. Ditmanson, and S. Bernet, "Discrete-time active damping of LCL-resonance by proportional capacitor current feedback," *IEEE Trans. Ind. Appl.*, vol. 50, no. 6, pp. 3911-3920, Nov. 2014.

[11] J. Dannehl, F. W. Fuchs, and S. Hansen, "PI state space current control

This article has been accepted for publication in a future issue of this journal, but has not been fully edited. Content may change prior to final publication. Citation information: DOI 10.1109/JESTPE.2018.2805823, IEEE Journal of Emerging and Selected Topics in Power Electronics

JESTPE-2017-09-0599.R1

11

of grid-connected PWM converters with LCL filters," *IEEE Trans. Power Electron.*, vol. 25, no. 9, pp.2320-2330, Sep. 2010.

[12] E. Wu, and P. W. Lehn, "Digital current control of a voltage source converter with active damping of LCL resonance," *IEEE Trans. Power Electron.*, vol.21, no. 5, pp. 1364–1373, Sep. 2006.

[13] M. Liserre, R. Teodorescu, and F. Blaabjerg, "Stability of photovoltaic and wind turbine grid-connected inverters for a large set of grid impedance values," *IEEE Trans. Power Electron.*, vol. 21, no. 1, pp. 263–272, Jan. 2006.

[14] J. Dannehl, C. Wessels, and F. Fuchs, "Limitations of voltage-oriented PI current control of grid-connected PWM rectifiers with LCL filters," *IEEE Trans. Ind. Electron.*, vol. 56, no. 2, pp. 380–388, Feb. 2009.

[15] J. Xu, S. Xie, and T. Tang, "Active damping based control for grid-connected LCL-filtered inverter with injected grid current feedback only," *IEEE Trans. Ind. Electron.*, vol. 61, no. 9, pp. 4746-4758, Sep. 2014.

[16] M. Hanif, V. Khadkikar, W. Xiao, and J. L. Kirtley, "Two degrees of freedom active damping technique for LCL filter based grid connected PV systems," *IEEE Trans. Ind. Electron.*, vol.61, no. 6, pp. 2795-2803, Jun. 2014.

[17] X. Wang, F. Blaabjerg, and P. C. Loh, "Grid-current-feedback active damping for LCL resonance in grid-connected voltage source converters," *IEEE Trans. Power Electron.*, vol. 31, no. 1, pp. 213-223, Jan. 2016.

[18] E. Wu, and P. W. Lehn, "Digital current control of a voltage source converter with active damping of LCL resonance," *IEEE Trans. Power Electron.*, vol.21, no.5, pp. 1364-1373, Sep. 2006.

[19] D. Pan, X. Ruan, and C. Bao, "Capacitor current feedback active damping with reduced computation delay for improving robustness of LCL-type grid-connected inverter," *IEEE Trans. Power Electron.*, vol. 29, no. 7, pp. 3414-3427, Jul. 2014.

[20] S. G. Parker, B. P. McGrath, and D. G. Holmes, "Regions of active damping control for LCL filters," *IEEE Trans. Ind. Appl.*, vol. 50, no.1, pp. 424-432, Jan. 2014.

[21] M. Liserre, R. Teodorescu, and F. Blaabjerg, "Stability of photovoltaic and wind turbine grid-connected inverters for a large set of grid impedance values," *IEEE Trans. Power Electron.*, vol. 21, no.1, pp. 263-272, Jan. 2006.

[22] J. Xu, S. Xie, and T. Tang, "Improved control strategy with grid-voltage feedforward for LCL-filter-based inverter connected to weak grid," *IET Power. Electron.*, vol. 7, no.10, pp. 2660-2671, Oct. 2014.

[23] I. J. Gabe, V. F. Montagner, and H Pinheiro, "Design and implementation of a robust current controller for VSI connected to the grid through an LCL filter," *IEEE Trans. Power Electron.*, vol. 24, no. 6, pp. 1444–1452, Jun. 2009.

[24] Y. A. I. Mohamed, and E. F. Saadany, "A robust natural-frame-based interfacing scheme for grid-connected distributed generation inverters," *IEEE Trans. Energy Convers.*, vol. 26, no. 3, pp. 728–736, Sep. 2011.

[25] J. M. E. Huerta, J. Castello, J. R. Fischer, and R. Garcia-Gil, "A synchronous reference frame robust predictive current control for three-phase grid-connected inverters," *IEEE Trans. Ind. Electron.*, vol. 57, no. 3, pp. 954-962, Mar. 2010.

[26] J. M. Espi, J. Castello, R. Garcı́a-Gil, G. Garcera, and E. Figueres, "An adaptive robust predictive current control for three-phase grid-connected inverters," *IEEE Trans. Ind. Electron.*, vol. 58, no. 8, pp. 3537-3546, Aug. 2011.

[27] L. Corradini, W. Stefanutti, and P. Mattavelli, "Analysis of multisampled current control for active filters," *IEEE Trans. Ind. Appl.*, vol. 44, no. 6, pp. 1785-1794, Nov. 2008.

[28] H. Deng, R. Qruganti, and D. Srinivasan, "PWM methods to handle time delay in digital control of a UPS inverter," *IEEE Trans. Power Electron.*, vol.3, no. 1, pp. 1-6, Mar. 2005.

[29] D. Yang, X. B. Ruan, and H. Wu, "A real-time computation method with dual sampling mode to improve the current control performance of LCL-Type grid-connected inverter," *IEEE Trans. Ind. Electron.*, vol. 62, no.7, pp. 4563 - 4572, Jul. 2015.

[30] Y. Chen, A. Luo, Z. K. Shuai, and S. Xie, "Robust predictive dual-loop control strategy with reactive power compensation for single-phase grid-connected distributed generation system," *IET Power Electron.*, vol. 6, no. 7, pp. 1320-1328, Aug. 2013.

Xiaoping Zhou (S'16) was born in Jiangxi, China, 1990. He received the B.S. degree in electrical engineering from Hunan University, Changsha, China, in 2013. Currently, he has been working toward the Ph.D. degree in electrical engineering from Hunan University, Changsha, China.

His research interests include power electronics converter, distributed generation, microgrid, power quality and energy storage.

Leming Zhou (M'17) was born in Hunan, China, in 1989. He received the B.S. and Ph.D. degree in electrical engineering from Hunan University, Changsha, China, in 2011 and 2016, respectively. Currently, he has been working postdoctoral research in electrical engineering from Hunan University, Changsha, China.

His research interests include power electronics, electric power green transformation, distributed generation, and marine special power supply.

Yandong Chen (S'13-M'14) was born in Hunan, China, in 1979. He received the B.S. and M.S. degree in instrument science and technology from Hunan University, Changsha, China, in 2003 and 2006, respectively, and the Ph.D. degree in electrical engineering from Hunan University, Changsha, China, in 2014.

His research interests include power electronics for microgrid, distributed generation, power quality, and energy storage. Dr. Chen is a recipient of the 2014 National Technological Invention Awards of China.

Zhikang Shuai (S'09-M'10-SM'17) received the B.S. and Ph.D. degree from the College of Electrical and Information Engineering, Hunan University, Changsha, China, in 2005 and 2011, respectively, all in electrical engineering. He was with the Hunan University, as an Assistant Professor between 2009 and 2012, and an Associate Professor in 2013. Starting in 2014, he became a Professor at Hunan University.

His research interests include power quality control, power electronics, and Microgrid stability analysis and control. Dr. Shuai is the Associate Editor of IEEE Journal of Emerging and Selected Topics in Power Electronics, Chinese Journal of Electrical Engineering. He is a recipient of the 2010 National Scientific and Technological Awards of China, the 2012 Hunan Technological Invention Awards of China, the 2007

Scientific and Technological Awards from the National Mechanical Industry Association of China.

Josep M. Guerrero (S'01-M'04-SM'08-FM'15) received the B.S. degree in telecommunications engineering, the M.S. degree in electronics engineering, and the Ph.D. degree in power electronics from the Technical University of Catalonia, Barcelona, in 1997, 2000 and 2003, respectively. Since 2011, he has been a Full Professor with the Department of Energy Technology, Aalborg University, Denmark. From 2015 he is a distinguished guest Professor in Hunan University.

His research interests mainly include power electronics, distributed energy-storage, and microgrids. Prof. Guerrero is an Associate Editor for the IEEE TRANSACTIONS ON POWER ELECTRONICS, the IEEE TRANSACTIONS ON INDUSTRIAL ELECTRONICS, and the IEEE Industrial Electronics Magazine, and an Editor for the IEEE TRANSACTIONS on SMART GRID and IEEE TRANSACTIONS on ENERGY CONVERSION. In 2014, 2015, and 2016 he was awarded by Thomson Reuters as Highly Cited Researcher, and in 2015 he was elevated as IEEE Fellow for his contributions on distributed power systems and microgrids.

An Luo (SM'09) was born in Changsha, China, in 1957. He received the B.S. and M.S. degrees in industrial automation from Hunan University, Changsha, in 1982 and 1986, respectively, and the Ph.D. degree in fluid power transmission and control from Zhejiang University, Hangzhou, China, in 1993. Between 1996 and 2002, he was a Professor with Central South University. Since 2003, he has been a Professor in the College of Electrical and Information Engineering, Hunan University. He was elected as academician of Chinese Academy of Engineering in 2015.

His research interests include distributed generation system, microgrid, power conversion, harmonics suppression and reactive power compensation, and electric power saving.

Wenhua Wu (S'16) was born in Hunan, China, 1991. He received the B.S. degree from the College of Electrical and Information Engineering, Hunan University, Changsha, China, in 2014. Currently, he has been working toward the Ph.D. degree in electrical engineering from Hunan University, Changsha, China.

His research interests include renewable energy generation systems, microgrid, power quality, and VSC-HVDC systems.

Ling Yang (S'16) was born in Liaoning, China, 1992. She received the B.S. degree from the College of Electrical and Information Engineering, Hunan University, Changsha, China, in 2014. Currently, she has been working toward the Ph.D. degree in electrical engineering from Hunan University, Changsha, China.

Her research interests include power electronics, and distributed power systems.